Article

Structure

A Structure-Based Strategy for Engineering Selective Ubiquitin Variant Inhibitors of Skp1-Cul1-F-Box Ubiquitin Ligases

Graphical Abstract

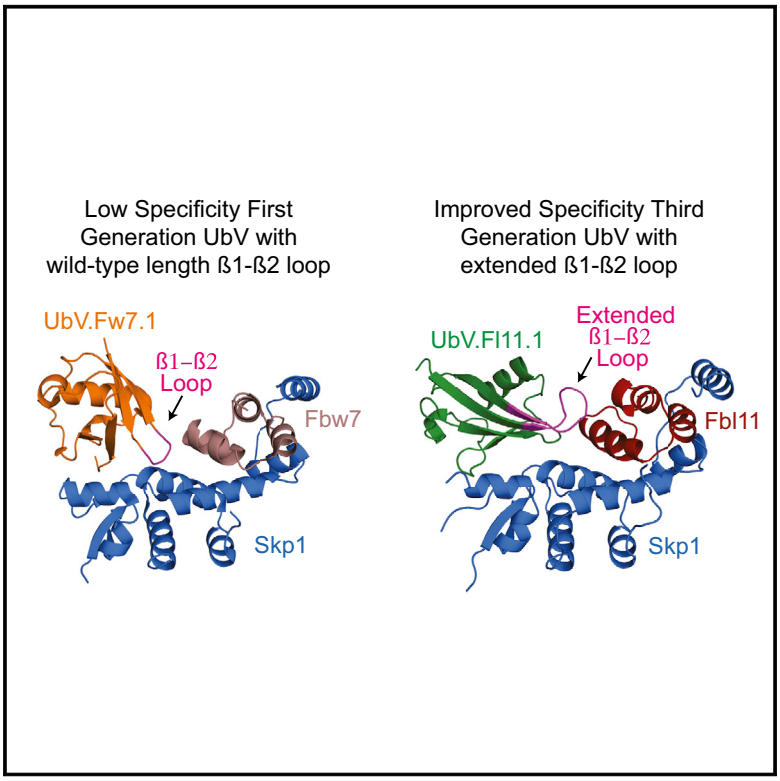

Highlights

- Ubiquitin variant (UbV) library designed to target specific F-box proteins
- Extended and varied UbV β1-β2 loop to improve specificity
- Selective UbV inhibitors generated against 17 F-box proteins using phage display
- 3 crystal structures show common UbV binding mode and β1-β2 loop contacts with F-box

Authors

Maryna Gorelik, Noah Manczyk, Alevtina Pavlenco, Igor Kurinov, Sachdev S. Sidhu, Frank Sicheri

Correspondence

sachdev.sidhu@utoronto.ca (S.S.S.), sicheri@lunenfeld.ca (F.S.)

In Brief

We used custom ubiquitin variant library to generate selective inhibitors against 17 different members of the SCF E3 ligase family. Structures of two representative ubiquitin variants in complex with their targets reveal details of the binding mechanism validating our approach and suggesting further improvements to the library design.

Gorelik et al., 2018, Structure *26*, 1226–1236
September 4, 2018
https://doi.org/10.1016/j.str.2018.06.004

CellPress

CellPress

Structure
Article

A Structure-Based Strategy for Engineering Selective Ubiquitin Variant Inhibitors of Skp1-Cul1-F-Box Ubiquitin Ligases

Maryna Gorelik,[1,2,6] Noah Manczyk,[3,4,6] Alevtina Pavlenco,[1] Igor Kurinov,[5] Sachdev S. Sidhu,[1,2,*] and Frank Sicheri[2,3,4,7,*]
[1]Banting and Best Department of Medical Research, Terrence Donnelly Center for Cellular and Biomolecular Research, University of Toronto, Toronto, ON M5S 3E1, Canada
[2]Department of Molecular Genetics, University of Toronto, Toronto, ON M5S 1A8, Canada
[3]Lunenfeld-Tanenbaum Research Institute, Mount Sinai Hospital, Toronto, ON M5G 1X5, Canada
[4]Department of Biochemistry, University of Toronto, Toronto, ON M5S 1A8, Canada
[5]Department of Chemistry and Chemical Biology, Cornell University, Argonne, IL 60439, USA
[6]These authors contributed equally
[7]Lead Contact
*Correspondence: sachdev.sidhu@utoronto.ca (S.S.S.), sicheri@lunenfeld.ca (F.S.)
https://doi.org/10.1016/j.str.2018.06.004

SUMMARY

Skp1-Cul1-F-box (SCF) E3 ligases constitute the largest and best-characterized family of the multisubunit E3 ligases with important cellular functions and numerous disease links. The specificity of an SCF E3 ligase is established by one of the 69 human F-box proteins that are recruited to Cul1 through the Skp1 adaptor. We previously reported generation of ubiquitin variants (UbVs) targeting Fbw7 and Fbw11, which inhibit ligase activity by binding at the F-box-Skp1 interface to competitively displace Cul1. In the present study, we employed an optimized engineering strategy to generate specific binding UbVs against 17 additional Skp1-F-box complexes. We validated our design strategy and uncovered the structural basis of binding specificity by crystallographic analyses of representative UbVs bound to Skp1-Fbl10 and Skp1-Fbl11. Our study highlights the power of combining phage display with structure-based design to develop UbVs targeting specific protein surfaces.

INTRODUCTION

Ubiquitin (Ub), a highly conserved 76-residue protein, is attached through the E1-E2-E3 enzymatic cascade in a variety of topologies to mark proteins for degradation or to alter their activity. Not surprisingly, the E3 ligases that control specificity of ubiquitination constitute the largest group with ~600 members in humans. Due to their large number and importance in controlling cellular fate, E3 ligases are considered important targets for therapeutic intervention.

Multisubunit Cullin RING ligases (CRLs) constitute the largest family of E3 ligases with ~250 members (Bhowmick et al., 2013) and are characterized by the presence of a Cullin subunit responsible for tethering a substrate receptor and a RING protein that, in turn, recruits E2-Ub. Seven distinct Cullin subunits (Cul1, Cul2, Cul3, Cul4A, Cul4B, Cul5, and Cul7) define seven CRL subfamilies, which also differ in terms of the type of substrate receptor (Skp1-F-box, EloBC-VHL, BTB, DDB1-DCAF, or EloBC-SOCS-box) and RING protein (Rbx1 and Rbx2) that are tethered (Bulatov and Ciulli, 2015). Skp1-Cul1-F-box (SCF) E3 ligases represent the best characterized CRL family, and they have attracted great attention because of their established and inferred roles in regulating diverse biological processes (reviewed in Zheng et al., 2016). In humans, 69 F-box proteins act as substrate receptors for SCF E3 ligases and are bound to the Cul1 subunit through the adaptor Skp1. Binding to Skp1 is mediated by a small F-box domain of 50 residues, which is similar in all F-box proteins (Zheng et al., 2002). F-box family members are divided into three subfamilies denoted Fbw, Fbl, and Fbo, based on the presence of an additional WD40, LRR, or "other" domain, respectively, which functions to recruit substrates.

Small-molecule inhibitors of individual SCF E3 ligases have been developed to disrupt substrate binding (Nangle et al., 2013; Chen et al., 2013; Wu et al., 2012; Orlicky et al., 2010) or the interaction between F-box and Skp1 (Aghajan et al., 2010; Chan et al., 2013). However, effective inhibitors are lacking for the vast majority of F-box proteins, and, thus, the biological effects and therapeutic potential of inhibiting their E3 ligase functions remain unexplored.

Protein-based modulators of enzymes can aid in the development of small-molecule therapeutics by assisting in target validation, by serving as probes in displacement screens, and by serving as leads for structure-based inhibitor design. The Ub scaffold is particularly amenable for protein engineering of variants that function as either inhibitors or activators. Ubiquitin variants (UbVs) that bind to a variety of target proteins have been generated through several different approaches (Lorey et al., 2014; Hoffmann et al., 2012; Zhang et al., 2013; Leung et al., 2017). Research by our group using a phage display method to generate UbVs has been successful in targeting diverse components of the ubiquitin proteasome system (UPS) including deubiquitinases (Ernst et al., 2013), UIMs (Manczyk et al., 2017), E2 enzymes (Ernst et al., 2013), HECT E3 ligases (Zhang et al., 2016),

RING and U-box E3 ligases (Gabrielsen et al., 2017), the anaphase promoting complex/cyclosome (APC/C) complex (Brown et al., 2016), and SCF E3 ligases (Gorelik et al., 2016).

Since many UPS enzymes use weak Ub-binding sites for their normal biological functions, it is not surprising that most UbVs are generated by the strengthening of these natural interactions. However, in the case of SCF E3 ligases, we identified a UbV that bound to a composite surface on the Skp1-Fbw7 subcomplex not previously known to interact with Ub. The UbV binding surface overlapped extensively with the binding surface on Skp1 for Cul1. Consequently, the UbV functioned as an inhibitor of SCF^{Fbw7} activity by disrupting Cul1 binding. This finding revealed a previously uncharacterized inhibitory site in SCF E3 ligases (Gorelik et al., 2016).

One attractive feature of targeting the Cul1 interacting surface of the Skp1-F-box subcomplex is that it affords a potentially general means to inhibit an SCF complex without any knowledge of substrates and substrate binding mechanisms of the F-box subunit, which remains poorly understood for most F-box proteins. However, the issue of specificity remains a potential liability to this strategy because the Cul1 binding surface is largely contained on the common Skp1 subunit. Indeed, in generating UbVs that bound to Skp1-Fbw7, we observed that our model UbV displayed cross-reactivity to several other Skp1-F-box complexes. By analyzing the co-structure of a UbV bound to Skp1-Fbw7, we confirmed that cross-reactivity stemmed from the UbV forming the majority of its contacts with the common Skp1 component while forming only a minority of contacts, notably involving the β1-β2 loop of the UbV, with the variable F-box component (Fbw7). Thus we hypothesized that specificity could be improved by increasing the contacts between the F-box and the β1-β2 loop. To this end, we increased the length of the β1-β2 loop and subjected it to random diversification (Gorelik et al., 2016). In doing so, we isolated a UbV with an extended β1-β2 loop that bound with high specificity to Fbw11, discriminating even against the highly related protein Fbw1.

Here we sought to determine if the β1-β2 loop diversification strategy is generalizable for generating specific UbV binders for a larger set of Skp1-F-box complexes, including members of Fbw, Fbl, and Fbo subfamilies. We generated UbV binders targeting 21 different Skp1-F-box complexes, and, among these, showed that UbVs targeting 17 complexes were highly specific. Furthermore, we solved structures of a representative high specificity UbV generated against $Skp1\text{-}F\text{-}box^{Fbl11}$ and a less-specific UbV generated against $Skp1\text{-}F\text{-}box^{Fbl10}$ in complex with their cognate targets. These structures describe binding mechanism employed by UbVs with extended β1-β2 loops and provide insight into the specificity determinants of UbV-F-box interactions. Together, our findings demonstrate that an F-box-targeted UbV library can be exploited to generate specific binders against F-box proteins on a large scale and suggest possible modifications to the library design for further improvements.

RESULTS

Binding Selections with an F-Box-Targeted Phage-Displayed UbV Library

Toward developing improved F-box-specific UbVs, we designed a phage-displayed library based on one that we employed in our previous study. In particular, we left the predicted Skp1 contacting residues in our UbV template fixed to those observed in a previously characterized Skp1-Fbw7 binder, UbV.Fw7.5, and varied the size and sequence of the β1-β2 loop. Our strategy for varying the β1-β2 loop differed slightly from our previous UbV library (Gorelik et al., 2016) by inserting 6–8 residues (rather than 7–9 residues) and by randomizing 10–12 residues (rather 11–13 residues) (Figure 1A). We found that by slightly decreasing the number of inserted residues in the β1-β2 loop, we increased the fraction of UbVs in the naive library that were displayed at high levels on phage (Figure S1).

We chose 32 human F-box family members as targets for UbV selections, including some with well-characterized biological functions and connections to disease (e.g., Fbl1 [Skp2], Fbw1 [β-TrcpA], and Fbo5 [Emi1]) and others with completely uncharacterized functions. We expressed each isolated F-box domain (see Table S1 for domain boundaries) in complex with Skp1. Of 32 F-box domains, 23 could be purified in complex with Skp1 for use in 4 rounds of binding selections with the F-box targeted phage-displayed UbV library (Figure 1B). Following selections, the binding of individual UbV-phage clones was tested by phage ELISA. Only those UbVs which met the following criteria were further characterized: (1) confirmed as binders with greater than 2-fold higher signal toward the target Skp1-F-box relative to GST; (2) showed some measure of specificity with greater than 2-fold higher signal toward the target Skp1-F-box relative to the reference standard Skp1-Fbw7; and (3) binding inhibited by Cul1 with greater than 20% reduction in binding signal in the presence of Cul1. We expected that these criteria would narrow the population of UbV binders to those that conformed to our design strategy and specifically targeted the Cul1 binding surface of a particular Skp1-F-box complex (Gorelik et al., 2016). Two Skp1-F-box complexes (Fbl13 and Fbl18) did not meet the first selection criterion and four complexes (Fbl6, Fbo24, Fbo28, and Fbl6) did not meet the second selection criterion, and, thus, 6 of the 23 purified complexes failed to generate UbVs selective for the target Skp1-F-box (Figure 1B).

Using the above criteria we succeeded in generating UbV binders with at least some evidence of specificity for 17 of the 23 purified Skp1-F-box complexes (Figure 1B; Table S1), representing a success rate of over 70%. The number of unique UbV binders obtained for each Skp1-F-box complex varied considerably (Figure 1C; Table S2). Fbl7, Fbl10, Fbo4, Fbo11, Fbo34, Fbo43, and Fbo45 yielded 6–18 unique UbVs each, which allowed us to define consensus motifs for the diversified positions (Figure 1D). Other selections yielded either fewer unique UbVs (<5) or highly variable UbV sequences, which precluded determination of consensus motifs.

Comparison of the unique UbV sequences for each Skp1-F-box complex revealed that only two UbVs (out of 128 total) were selected by more than one (in this case two in total) F-box proteins. In one case, UbV.Fo5/43.1 was selected as one of three or one of seven unique UbVs by Fbo5 (Emi1) or Fbo43 (Emi2), respectively (Table S2). While these two F-boxes exhibit 44% sequence identity (Figure 2A), and thus represent two of the more similar proteins in our study, two even more similar F-boxes, namely Fbl10 (Kdm2b) and Fbl11 (Kdm2a) (67% identity; Figure 2A), selected distinct UbV sequences.

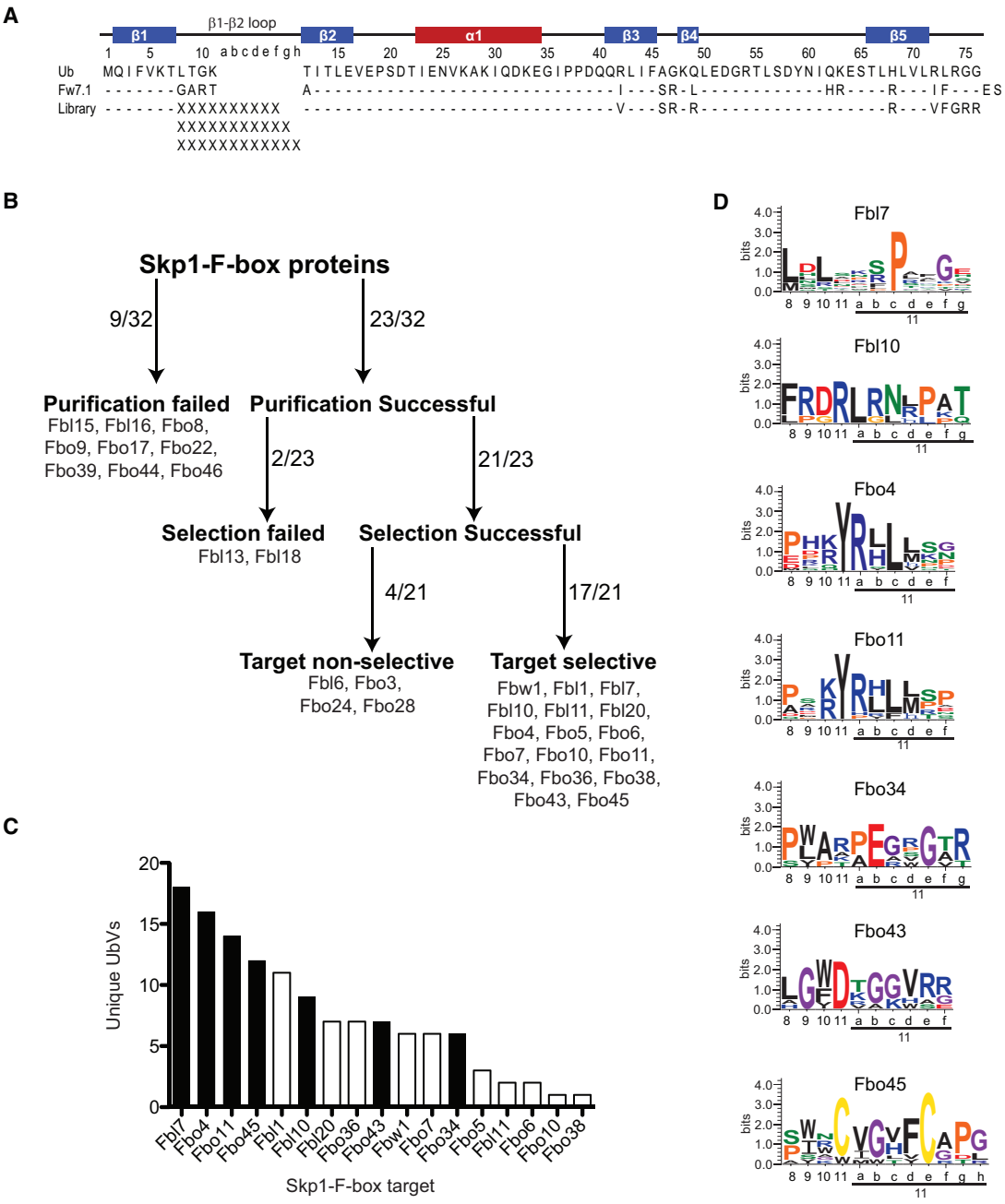

Figure 1. Selection of Phage-Displayed UbVs Targeting a Panel of Human F-Box Proteins

(A) F-box-targeted UbV library design. The sequence of wild-type (WT) Ub is shown and UbV positions conserved as WT are indicated by dashes. Positions that were fixed in UbV.Fw7.1 or the library but differ from WT are shown. Each position that was diversified in the library is indicated by an "X," which represents all 20 amino acids encoded by a degenerate NNK codon (N = A/G/C/T, K = G/T). Three sub-libraries were made with insertions of 6, 7, or 8 codons between positions 11 and 12, and these were combined to generate the final library used for selections.

(B) Summary of Skp1-F-box protein purification and UbV selection results. The targeted F-box proteins are shown as follows: phage selections generated UbVs against the F-box target, "Selection successful"; generated UbVs demonstrated preference for the target Skp1-F-box complex (>2-fold higher signal to target Skp1-F-box versus Skp1-Fbw7 in phage ELISA), "Target selective"; generated UbVs showed no preference for the target Skp1-F-box complex (<2-fold higher signal to target Skp1-F-box versus Skp1-Fbw7 in phage ELISA), "Target non-selective"; phage selections failed to produce UbVs against the F-box target, "Selection failed"; Skp1-F-box complexes could be purified at sufficient quantities for the use in phage selections and ELISAs, "Purification successful"; Skp1-F-box complexes could not be purified, "Purification failed."

(C) Number of unique binding UbVs generated for each Skp1-F-box complex. Black bars indicated targets for which UbVs exhibited a clear consensus sequence in the diversified β1-β2 loop.

(D) Sequence logos (generated by WebLogo [Crooks et al., 2004]) for the diversified residues in the β1-β2 loop of unique UbVs selected for binding to the indicated Skp1-F-box complexes.

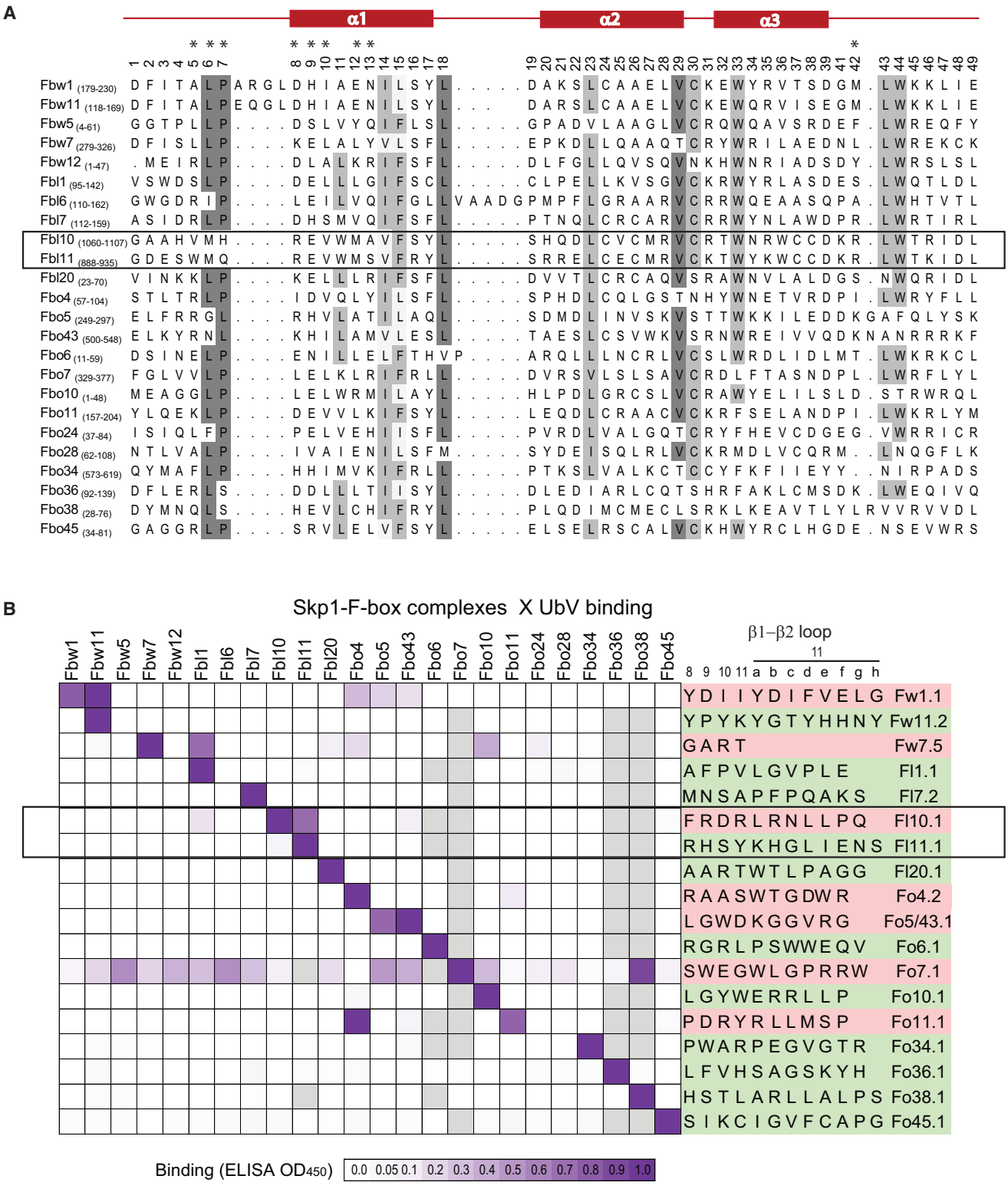

Figure 2. Binding Specificities of Phage-Displayed UbVs

(A) Sequence alignment of the 69 human F-box domains. The F-box domains were aligned based on the available F-box structures and conservation calculated at each position (see the STAR Methods). Residues with >75% conservation and >50% conservation are shaded dark gray or light gray, respectively. Only 24 F-box domains included in the UbV binding specificity analysis are shown. Asterisks (*) indicate F-box domain positions involved in UbV interactions based on the structures of UbVs in complex with Skp1-Fbl11 or Skp1-Fbl10.

(legend continued on next page)

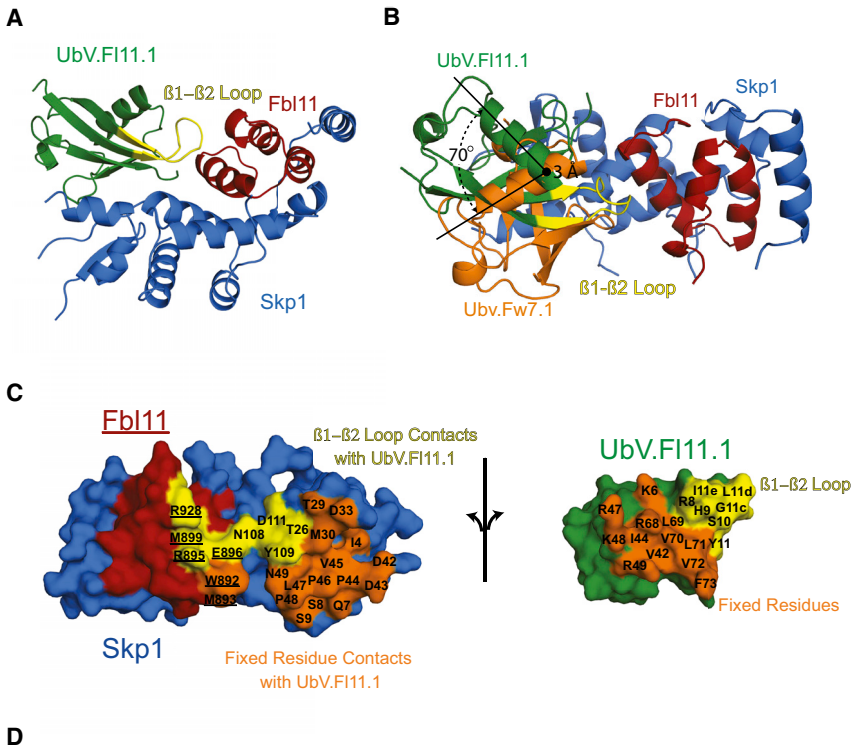

Figure 3. The Crystal Structure of UbV.Fl11.1 Bound to Skp1-Fbl11

(A) Overall architecture of the UbV.Fl11.1-Skp1-Fbl11 complex.

(B) The structures of UbV.Fl11.1-Skp1-Fbl11 and UbV.Fw7.1-Skp1-Fbw7 superimposed by their Skp1 subunits. The rotation axis, rotation angle, and translation required to superimpose UbV.Fw7.1 onto UbV.Fl11.1 are shown. Translation is occurring outward from PAGE.

(C) Open book view of the contact surfaces between UbV.Fl11.1 and Skp1 and Fbl11. Skp1 and Fbl11 residues engaged by the β1-β2 loop of UbV.Fl11.1 are colored yellow and those engaged by UbV.Fl11.1 residues that were fixed in the library are colored orange. Residues that contact both the β1-β2 loop and the fixed residues are colored based on which part of UbV.Fl11.1 they form the majority of their contacts with. Unengaged surfaces of Skp1 are colored blue and unengaged surfaces of Fbl11 are colored red. The UbV.Fl11.1 β1-β2 loop and core residues engaged in the interaction with the Skp1-Fbl11 complex are colored yellow or orange, respectively. Unengaged surfaces on Ubv.L11 are colored green.

(D) Details of the molecular interactions between UbV.Fl11.1 and Fbl11. Dashed lines indicate hydrogen bonds.

Asterisks indicate residues from UbV.Fl11.1.

Specifically, Fbl10 selected multiple UbVs that shared a motif (Figure 1D), whereas Fbl11 strongly selected (95% of all clones sequenced) a distinct UbV (Table S2). This result suggested that sequence diversity across the F-box family may be sufficient to generate distinct binding preferences, an issue explored further below. In the second case, two of the more dissimilar F-boxes, Fbo4 and Fbo11 (36% identify; Figure 2A), both selected UbV.Fo11.1 (Table S2) and families of UbVs with similar consensus motifs (Figure 1D).

Characterization of UbV Binding Specificity

To investigate specificity in greater detail, we assessed binding of the selected UbVs for the various Skp1-F-box complexes by phage ELISAs. For each Skp1-F-box complex, we chose up to three UbVs for characterization based on prioritization of binding strength, clone abundance in the selected pool, and sequence diversity. We measured the binding signals of 29 unique UbV-phage across a panel of 19–24 immobilized Skp1-F-box complexes. Figure 2B shows the most specific UbV for each of the Skp1-F-box complexes, while Figure S2 shows specificity data for all 29 UbVs that were tested. Providing corroboration that the selection process does impart significant specificity, 27 of 29 UbVs bound to their cognate target with the highest binding signal (Figures 2B and S2). The two exceptions were UbVs selected for binding to Fbw1, which exhibited higher binding signals to the closely related Fbw11 (89% identity; Figures 2B and S2).

We classified UbVs as monospecific if they displayed >10-fold higher binding signal toward their target relative to every other Skp1-F-box tested. Based on this definition, we generated monospecific UbVs for 11 of the 17 Skp1-F-box complexes that yielded specific binders (Figure 2B). UbV.Fw11.2, which targets Fbw11, was previously shown to be highly selective when tested against six other Skp1-F-box complexes (including the highly related Fbw1, 89% identity) (Gorelik et al., 2016). When assayed here for binding to 21 Skp1-F-box complexes, it exhibited absolute specificity for Fbw11. Monospecificity was also exhibited by UbV.Fl11.1,

(B) Phage ELISA binding specificities of the 17 most specific UbVs targeting 17 different Skp1-F-box complexes. For the Skp1-F-box targets with more than one characterized UbV, the UbV with the highest specificity is shown. See Figure S2 for the specificity profiles of all 29 characterized UbVs. Binding of phage-displayed UbV to immobilized Skp1-F-box complexes was detected spectrophotometrically and the absorbance at 450 nM is shown normalized to the signal for cognate Skp1-F-box complex. Gray boxes indicate interactions that were not assayed. The UbV.Fw7.5 and UbV.Fw11.2, targeting Fbw7 or Fbw11, respectively, were described previously (Gorelik et al., 2016). UbVs classified as specific (normalized binding to all non-cognate Skp1-F-box complexes <0.1) are shaded green, and the remaining UbVs with different degrees of cross-reactive behavior are shaded red.

Table 1. Crystallographic Data Collection, Processing, and Refinement Statistics

	UbV.Fl11.1-Skp1-Fbl11	UbV.Fl10.1-Skp1-Fbl10	UbV.Fl10.1-Skp1-Fbl11
Data Collection			
Space group	$P2_12_12_1$	$P2_12_12_1$	$P2_1$
Wavelength (Å)	1.54	0.979	0.979
Cell dimension			
a, b, c (Å)	60.6, 118.2, 146.3	65.4, 81.8, 128.7	38.2, 119.6, 63.7
α, β, γ (°)	90, 90, 90	90, 90, 90	90, 98.5, 90
Resolution range (Å)	50–2.61	50–2.66	19.82–3.27
R_{sym}	0.102 (1.00)	0.174 (1.07)	0.179 (1.07)
CC½	(0.864)	(0.781)	(0.547)
Total no. of observations	218,630	109,832	31,378
Total no. of unique observations	32,211 (2,735)	20,716 (2,028)	8,718 (1,811)
Mean [(I)/σ(I)]	24.7 (1.7)	16.5 (2.15)	5.2 (1.1)
Completeness (%)	98.5 (85.4)	99.8 (99.9)	98.9 (99.3)
Multiplicity	6.8 (5.2)	5.3 (4.6)	3.6 (3.5)
Refinement			
Resolution (Å)	43.4–2.61	47.5–2.66	19.82–3.27
No. of reflections	31,608	20,406	8,658
R_{work}/R_{free}	23.7/29.4	21.6/26.3	26.0/31.7
No. of atoms			
Protein	6,166	4,071	3,529
Ligand/ion	0	0	0
Water	70	40	0
Average B factors			
Protein	66.88	69.54	91.84
Ligand/ion	NA	NA	NA
Water	51.17	49.33	NA
RMSD			
Bond length (Å)	0.006	0.006	0.003
Bond angles (°)	0.799	0.881	0.615
Ramachandran statistics (%)			
Residues in favored regions	95.21	96.39	95.06
Residues in allowed regions	4.66	3.61	4.94
Residues in disallowed regions	0.13	0	0

Statistics in parentheses are for highest-resolution shell. NA, not applicable; RMSD, root-mean-square deviation.

which was selected for binding to Skp1-Fbl11 and did not bind appreciably even to the closely related Skp1-Fbl10 (67% identity in the F-box domains). UbVs exhibiting monospecificity were also isolated for Skp1 in complex with Fbl1, Fbl7, Fbl20, Fbo6, Fbo10, Fbo34, Fbo36, Fbo38, or Fbo45.

For two pairs of Skp1-F-box complexes, the selections yielded bispecific UbVs. UbVs selected for binding to Skp1-Fbo4 or Skp1-Fbo11 exhibited similar sequences (Figure 1D) and recognized both complexes. In the case of the Fbo5 and Fbo43 complexes, which share high sequence homology (44% identity in the F-box domain) and biological functions, the same UbV.Fo5/43.1 was the most specific and it recognized both complexes but no others. UbV.Fbl10.1, which was selected for binding to Fbl10, bound most strongly to its target Skp1-Fbl10 and to the similar Skp1-Fbl11 (67% identity in the F-box domain), but also bound weakly to several other Skp1-F-box complexes. Finally, the most specific UbVs selected for binding to Skp1-Fbw1 (UbV.Fw1.1), Skp1-Fbw7 (UbV.Fw7.5) (Gorelik et al., 2016) or Skp1-Fbo7 (UbV.Fo7.1), exhibited significant binding to several complexes beyond the expected targets (Figure 2B). Taken together, these results demonstrate that extension and diversification of the β1-β2 loop enabled the selection of absolutely or highly selective UbVs for the majority of Skp1-F-box complexes that we targeted.

Structural Analysis of UbVs Bound to Skp1-Fbl11 and Skp1-Fbl10 Complexes

We previously elucidated the structure of UbV.Fw7.1 bound to Skp1-Fbw7 (PDB: 5IBK). However, we lacked a structural understanding of the mechanism of action of UbVs bearing extended β1-β2 loops designed to favor particular Skp1-F-box complexes. Thus, to better understand the molecular basis for specificity and to confirm our design strategy, we chose representative examples of highly specific (UbV.Fl11.1) and less specific (UbV.Fl10.1) UbVs for structural analysis.

We solved the structure of UbV.Fl11.1 bound to Skp1-Fbl11 to 2.61 Å resolution by molecular replacement (Figure 3A; see the STAR Methods and Table 1 for data collection and structure refinement statistics). The crystal asymmetric unit consisted of three highly similar (average root-mean-square deviation [RMSD] = 0.28 Å) trimeric complexes, and as such we focused our description on a single complex (chains B, F, and H) (Figure S3A). The binding mode of UbV.Fl11.1 to Skp1-Fbl11 was similar in some respects to the binding mode of UbV.Fw7.1 to Skp1-Fbw7 (Figure 3B). UbV.Fl11.1 targeted a very similar Cul1 binding surface on the Skp1-F-box complex and the total surface areas buried by the UbVs were similar (1,913 $Å^2$ for UbV.Fl11.1 and 1,738 $Å^2$ for Ubv.Fw7.1). Despite sharing a common binding surface on the Fbl11-Skp1 complex, UbV.Fl11.1 bound in a strikingly different orientation relative to UbV.Fw7.1 (a 70° rotation and a 3 Å translation of the UbVs) (Figure 3B). The change in binding orientation of UbV.Fl11.1 relative to UbV.Fw7.1 may be caused by one or a combination of the following factors (see also Figure S4 for a detailed illustration of differences between the two UbVs originating from three successive engineering cycles): (1) the eight residue insertion within the β1-β2 loop of UbV.Fl11.1; (2) nine substitutions outside the β1-β2 loop that UbV.Fl11.1 contains relative to UbV.Fw7.1, which were incorporated to improve Skp1 binding (A12T, I42V, L49R, H62Q, K63R, I72V, R74G, G75R, and G76R, substitutions are written as UbV.Fw7.1 to UbV.Fl11.1); (3) the presence of Skp1 acidic loops in the Skp1-Fbl11-UbV.Fl11.1 complex that were shortened in the Skp1-Fbw7-Ubv.Fw7.1 complex (Schulman et al., 2000); and (4) the two extra C-terminal residues on UbV.Fw7.1 relative to UbV.Fl11.1. It is not readily

Table 2. Mutational Analysis of Fbl10 and Fbl11 Binding to Target UbVs

	IC_{50} (nM)[a]					
	Fbl11	Fbl11 W892V	Fbl10	Fbl10 V1064W	Fbl10 V1069A	Fbl10 A1072Y
UbV.Fl11.1	79 ± 11	690 ± 110	870 ± 80	71 ± 10		
UbV.Fl10.1	430 ± 30		140 ± 11		220 ± 30	22 ± 1.4

See also Figure 4 for isothermal titration calorimetry of UbV.Fl11.1 binding to Skp1-Fbl11 and UbV.Fl10.1 binding to Skp1-Fbl10 and Skp1-Fbl11.
[a]IC_{50} values were calculated by competitive ELISA as the concentration of Skp1-F-box in solution that blocked 50% of UbV binding to immobilized Skp1-F-box complexes. Values represent mean ± SD.

apparent which of these changes are responsible for the altered binding modes of the two UbVs.

Consistent with the library design, the extended β1-β2 loop of Ubv.Fl11.1 engaged the F-box domain, and, furthermore, the surface area buried between UbV.Fl11.1 and the Fbl11 F-box subunit (Figure 3C) was increased greatly relative to that between UbV.Fw7.1 and the Fbw7 F-box (727 and 322 $Å^2$, respectively). In particular, the β1-β2 loop of UbV.Fl11.1 formed the majority of the contacts with Fbl11 (~75% of the buried surface area), but other residues that were fixed in the library design also contributed to the interaction. Contacts with the F-box mediated in part by the extended β1-β2 loop included both hydrophobic and hydrogen bond interactions, and provided a likely basis for the specificity of the UbV. Specifically, hydrophobic residues Trp892 and Met893 on Fbl11 interacted with UbV residues Tyr11*, Leu71*, and Phe73*, while Met899 on Fbl11 interacted with Leu11d* (UbV residues are indicated by "*" and insertions relative to the Ub sequence are indicated by lower case letters) (Figure 3D, left panel and detailed stereo view in Figure S5, top panel). Hydrogen bond interactions involved the side chain of Trp892 with the side chain of Gln40* and backbone oxygen of Val72* (Figure 3D, left panel), the side chain of Arg895 with the main chain oxygens of Ser10*, Tyr11*, and His11b*, the side chain of Arg928 with the main chain oxygen of His11b* (Figure 3D, center panel), and the side chain of Glu896 with the side chain of Ser10* (Figure 3D, right panel).

Notably, among all the contact residues on Fbl11, only Trp892 (Val1064 in Fbl10) differed from the corresponding residues in Fbl10, but, nonetheless, Fbl10 exhibited only weak binding to UbV.Fl11.1. Trp892 makes contacts with residues both within and outside of the β1-β2 loop (Figure 3D left panel and Figure S5 top panel). The smaller side chain of Val1064 in Fbl10 relative to Trp892 in Fbl11 would likely make suboptimal packing contacts with a loss of hydrogen bond interactions (Figure S5, bottom panel). Thus, it appears that Trp892 is a key determinant of the specificity of UbV.Fl11.1 for Skp1-Fbl11 over Skp1-Fbl10. To test this hypothesis we substituted Val for Trp at position 892 in Fbl11 and Trp for Val at position 1064 in Fbl10 and tested each for binding to UbV.Fl11.1 (Table 2) using a competitive protein ELISA. In this assay Skp1-Fbl11 displayed a half maximal inhibitory concentration (IC_{50}) of 79 nM against UbV.Fl11.1, similar to the K_D of 25 nM measured by isothermal titration calorimetry (ITC) (Figure 4, left panel). Consistent with the preference for Fbl11 demonstrated by phage ELISA (Figure 2B), UbV.Fl11.1 bound Fbl11 with ~10-fold greater affinity relative to Fbl10 (Table 2). Confirming our prediction that Trp892 specifies preferential binding of UbV.Fl11.1 to Fbl11, the Fbl11 variant with a W892V substitution displayed reduced binding comparable with that of Fbl10, and, conversely, the Fbl10 variant with a V1064W substitution displayed increased binding comparable with that of Fbl11 (Table 2).

We also used molecular replacement to solve the structure of UbV.Fl10.1 bound to each of its two strongest binding partners, Skp1-Fbl10 and Skp1-Fbl11, at 2.66 and 3.27 Å resolution, respectively (Figure 5A; see the STAR Methods and Table 1 for data collection and structure refinement statistics). Both crystal asymmetric units consisted of two highly similar trimeric complexes (RMSD = 0.35 Å for UbV.Fl10.1-Skp1-Fbl10 and RMSD = 0.95 Å for UbV.Fl10.1-Skp1-Fbl11), and, as such, we focused our descriptions on a single complex for each structure (chains A, C, and F and chains A, C, and H, respectively; Figures S3B and S3C). The overall binding modes of UbV.Fl10.1 to Skp1-Fbl10 and to Skp1-Fbl11 were highly similar to each other and to the binding mode of UbV.Fl11.1 to Skp-Fbl11, with only small differences in center of mass positions and rotations (Figure S6). Thus, in all three UbV structures with extended β1-β2 loops, the UbVs bound to Skp1-F-box complexes with very similar orientations that were distinct from that of UbV.Fw7.1 with a short β1-β2 loop.

The surfaces between UbV.Fl10.1 and Skp1-Fbl10 or Skp1-Fbl11 were highly overlapping with contact areas of 2,078 and 1,724 $Å^2$, respectively (Figure 5B). Consistent with the lower specificity of UbV.Fl10.1 relative to UbV.Fl11.1 (Figure 2B), UbV.Fl10.1 had a smaller contact surface with Fbl10 (336 $Å^2$) or Fbl11 (344 $Å^2$) than did UbV.Fl11.1 with Fbl11 (727 $Å^2$).

Among F-box residues that contact UbV.Fl10.1 and thus may contribute to binding specificity, Val1069 and Ala1072 in Fbl10, and the corresponding Val897 and Ser900 in Fbl11, differ in other F-box proteins that bind weakly to UbV.Fl10.1 (Figures 5C and 2A). These side chains in the F-box appear to allow efficient packing against Leu11a* in UbV.Fl10.1 (Figure 5C). In contrast, the weak binding F-box proteins have bulkier residues at the position corresponding to Ala1072/Ser900 and/or contain a residue other than valine at the position corresponding to Val1069/Val897. To test whether these two positions dictate the preference of UbV.Fl10.1 for Fbl10 and Fbl11 over other F-box proteins, we assessed the effect of V1069A (Ala representing an amino acid different than the conserved Val) and A1072Y (Tyr representing a bulkier side chain compared with Ala/Ser) substitutions in Fbl10 on Ubv.Fl10.1 binding using the competitive protein ELISA. In this assay, Skp1-Fbl10 exhibited an IC_{50} of 140 nM against UbV.Fl10.1, and Skp1-Fbl11 exhibited an IC_{50} of 430 nM

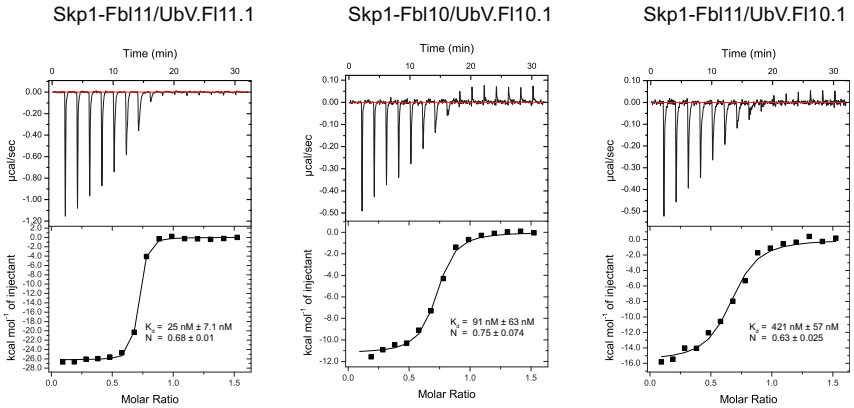

Figure 4. Isothermal Titration Calorimetry Analysis of UbV.Fl11.1 Binding to Skp1-Fbl11, UbV.Fl10.1 Binding to Skp1-Fbl10, and UbV.Fl10.1 Binding to Skp1-Fbl11

See the STAR Methods for experimental details. Experiment performed in triplicate. Values represent mean ± SD.

against Skp1-Fbl11 (Table 2), similar to the K_d of 91 or 421 nM, respectively, measured by ITC (Figure 4, middle and right panels). Contrary to our hypothesis, the Fbl10 V1069A substitution did not decrease binding considerably, while the Fbl10 A1072Y substitution actually increased binding (Table 2). Thus the basis for the specificity of UbV.Fl10.1 for Skp1-Fbl10 and Skp1-Fbl11 remains an open question.

Effects of UbVs on the Function of SCF^{Fbl1} and SCF^{Fbo11} in Cells

To test whether UbVs are able to inhibit SCF E3 ligases in cells, we chose UbV.L1.1 and UbV.O11.1 targeting SCF^{Fbl1} and SCF^{Fbo11}, respectively, for testing in HEK293T cells. SCF^{Fbl1} (Skp2) is one of the best characterized SCF E3 ligases and is considered an important oncogene with numerous studies attempting to engineer SCF^{Fbl1} inhibitors for cancer treatment (Skaar et al., 2014). SCF^{Fbo11} is also well characterized and, along with SCF^{Fbl1}, has been shown to be among the most abundant SCF ligases in HEK293T cells (Reitsma et al., 2017). To determine whether cellular expression of UbV.Fl1.1 or UbV.Fo11.1 could inhibit their cognate ligases, we analyzed the stability of ligase substrates. Consistent with anticipated inhibitory effects, UbV.Fl1.1 stabilized the SCF^{Fbl1} substrate p27, whereas UbV.O11.1 stabilized the SCF^{Fbo11} substrate Snail1 (Figures 6A and 6B) (Jin et al., 2015; Zheng et al., 2014). The observed effect was specific, as we did not observe any stabilization of substrates targeted by other SCF E3 ligases including cyclin E (Fbw7 substrate) and Cry2 (Fbxl3 substrate) in the case of UbV.L1.1 and cyclin E, Cry2 and c-Myc (Fbw7 and other E3 ligase substrate) in the case of UbV.O11.1 (Figures 6A and 6B). Taken together with the results of our previous study (Gorelik et al., 2016), which demonstrated inhibition of cellular SCF^{Fbw7} and SCF^{Fbw11} by UbVs, these results confirm that UbVs can target Cul1 binding sites on SCF E3 ligases to inhibit their functions in cells.

DISCUSSION

We previously reported a strategy to develop specific UbV inhibitors of SCF E3 ligases using the well-characterized F-box proteins Fbw7 and Fbw11 as test cases (Gorelik et al., 2016). Here we applied this approach to approximately half of the human F-box family by attempting to target 32 of the 69 members (Figure 1B). We successfully purified 23 of the 32 F-box domains in complex with Skp1, and for 17 of these we generated UbV binders with at least some level of specificity. Our results demonstrate that our strategy can generate fairly specific UbV inhibitors for a large majority of stable Skp1-F-box complexes that can be purified by recombinant expression in bacteria. Further improvements in this success rate should be achievable by optimization of the bacterial Skp1-F-box expression system or by using eukaryotic expression systems that are better able to support the correct folding of Skp1-F-box complexes.

A survey of binding specificities across a large panel of Skp1-F-box proteins (Figure 2B) revealed that many UbVs display high specificity for their cognate targets. Notably, for 11 Skp1-F-box complexes, we identified at least one monospecific UbV, and for four others, we identified bispecific UbVs. We designed the F-box-targeted UbV library with the expectation that extension and diversification of the β1-β2 loop would yield UbV binders with improved specificity through expanded and optimized interactions with the F-box domain. Consistent with our design, the β1-β2 loop of the highly specific UbV.Fl11.1 forms extensive interactions with the Fbl11 F-box domain (Figures 3C and 3D). The structures reported in this study of UbVs bound to Skp1-F-box complexes reveal that Gln40*, Leu71*, Val 72*, and Phe73*, which were fixed in the library design, make contacts with the F-box domain (Figures 3D and 5C) that were prohibited by distance constraints in the original structure of UbV.Fw7.1 bound to Skp1-Fbw7. We posit that these positions may be fertile ground for additional sequence diversification to further optimize specificity and affinity.

Although we have focused our efforts on developing UbV inhibitors for SCF E3 ligases, targeting other CRL families is also of a great interest. While the approach described here is not directly applicable to Cul4A and Cul4B families, since their substrate receptors do not interact directly with Cullin subunits (Angers et al., 2006), it could likely be applied to the other three CRL subfamilies. Namely EloBC-VHL-Cul2, EloBC-SOCs-box-Cul5, and BTB-Cul3 families not only share a common architecture with the SCF E3 ligases, they also share a structurally conserved interaction interface with Cul1 (Stogios et al., 2005) (Figure S7). As in the case of SCF E3 ligases, UbV inhibitors of these CRL families could be generated by targeting a defined and relatively small component that is responsible for the interaction with a Cullin subunit, without any knowledge of the overall structure or function. This strategy may be most successful for the BTB-Cul3 family, which is distinct in that BTB proteins interact with Cul3 directly, limiting the issue of specificity that arises when a common component such as

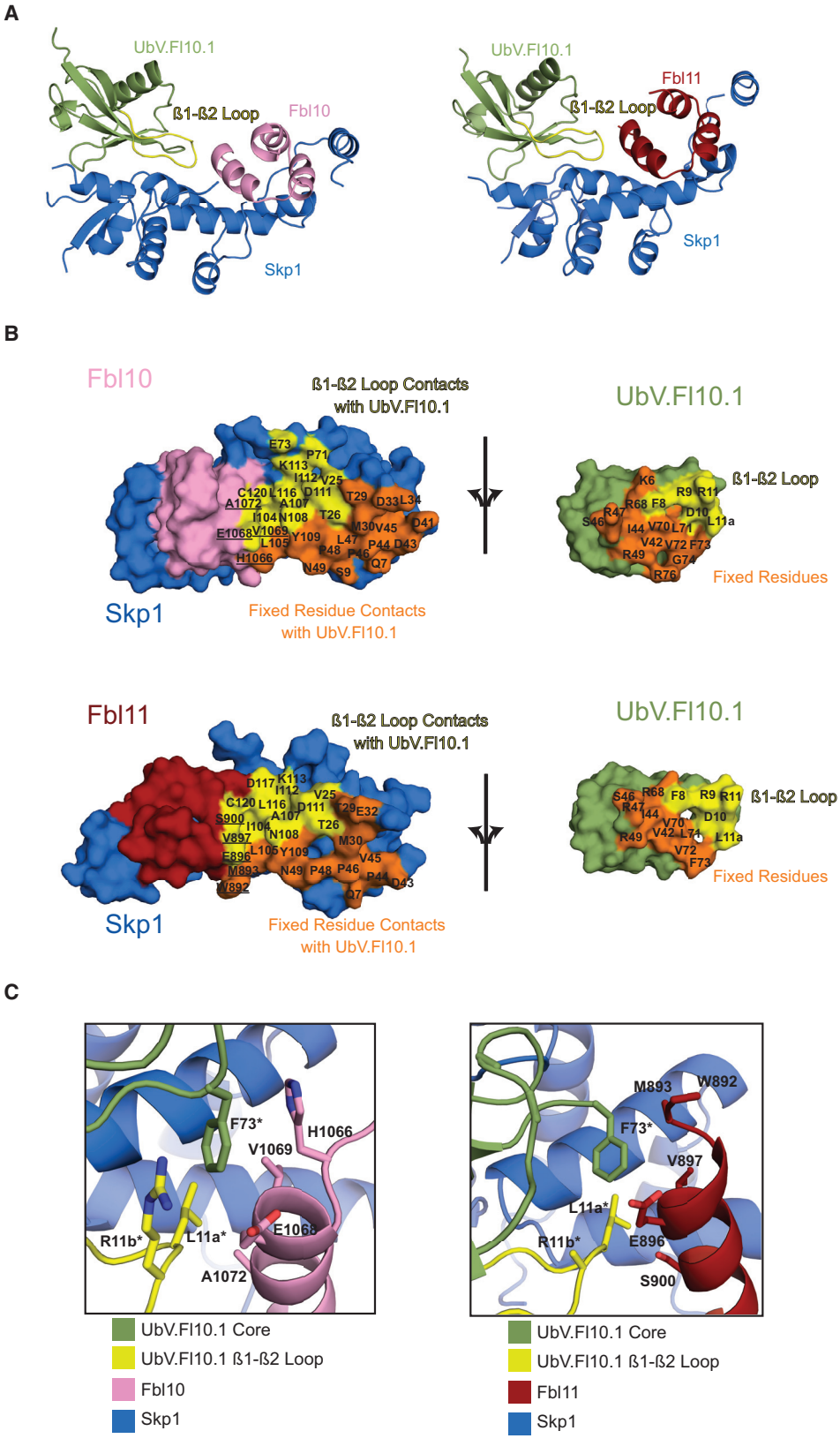

(legend on next page)

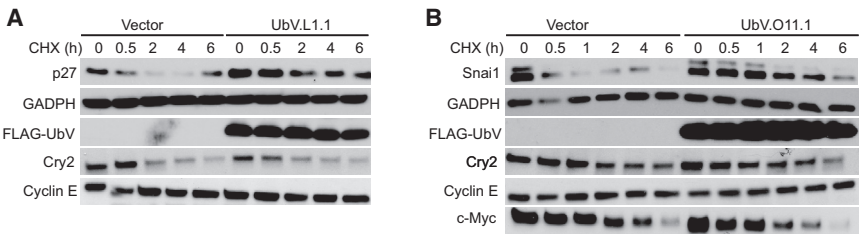

Figure 6. Biological Activity of UbVs in HEK293T Cells

(A) Expression of UbV.Fl1.1 stabilizes the SCF^{Fbl1} substrate p27, but has no effect on stability of the SCF^{Fbw7} substrate cyclin E and the SCF^{FbxL3} substrate Cry2. Cells were transiently transfected with either empty vector or vector encoding FLAG-UbV.Fl1.1. Cells were treated with 100 μg/mL cycloheximide (CHX) for the indicated time points and cell lysates were probed with antibodies against endogeneous p27, cyclin E, Cry2, GADPH (loading control), or FLAG (UbV levels).

(B) Expression of UbV.O11.1 stabilizes the SCF^{Fbo11} substrate Snai1 but has no effect on the stability of the SCF^{Fbw7} substrate cyclin E, the SCF^{FbxL3} substrate Cry, and the $SCF^{Fbw7,Skp2}$ substrate c-Myc. Cells were transiently transfected with hemagglutinin-tagged Snai1 and either empty vector or vector encoding FLAG-UbV.Fo11.1. Cells were treated with 20 μg/mL CHX for the indicated time points and cell lysates were probed with antibodies against Snail1, cyclin E, Cry2, c-Myc, GADPH (loading control), or FLAG (UbV levels).

Skp1 contributes to the targeted interaction surface. Most importantly, previous UbV inhibitors of Fbw7 and Fbw11 (Gorelik et al., 2016) and the UbVs described here can serve as useful tools to interrogate functions of SCF E3 ligases. Thus, we are well positioned to apply the UbV strategy to systematically develop specific inhibitors to a significant fraction of the large CRL family of E3 ligases.

STAR★METHODS

Detailed methods are provided in the online version of this paper and include the following:

- KEY RESOURCES TABLE
- CONTACT FOR REAGENT AND RESOURCE SHARING
- EXPERIMENTAL MODEL AND SUBJECT DETAILS
  - Protein Expression
  - Cell Based Assays
- METHOD DETAILS
  - Protein Expression and Purification
  - Library Construction and Binding Selections
  - ELISAs
  - Cell-Based Assays
  - F-box Alignment
  - Crystallization and Structure Determination
  - Isothermal Calorimetry
- QUANTIFICATION AND STATISTICAL ANALYSIS
  - Competitive ELISA Assays
  - Isothermal Calorimetry Assays
- DATA AND SOFTWARE AVAILABILITY
  - Accession Numbers

SUPPLEMENTAL INFORMATION

Supplemental Information includes seven figures and two tables and can be found with this article online at https://doi.org/10.1016/j.str.2018.06.004.

ACKNOWLEDGMENTS

This work was supported by Canadian Institutes of Health Research (CIHR) grants FDN 143277 to F.S., MOP-136956 to S.S., a CIHR postdoctoral fellowship to M.G., and an OSOTF award to N.M. This work is based upon research conducted at the Northeastern Collaborative Access Team beamlines, which are funded by the National Institute of General Medical Sciences from the NIH (P41 GM103403). The Pilatus 6M detector on 24-ID-C beamline is funded by a NIH-ORIP HEI grant (S10 RR029205). This research used resources of the Advanced Photon Source, a U.S. Department of Energy (DOE) Office of Science User Facility operated for the DOE Office of Science by Argonne National Laboratory under contract no. DE-AC02-06CH11357.

AUTHOR CONTRIBUTIONS

M.G. and N.M. designed and conducted the experiments and wrote the paper. A.P. and I.K. conducted the experiments. S.S.S. and F.S. designed the experiments and wrote the paper.

DECLARATION OF INTERESTS

The authors declare no competing interests.

Received: January 9, 2018
Revised: April 23, 2018
Accepted: June 8, 2018
Published: July 19, 2018

REFERENCES

Adams, P.D., Afonine, P.V., Bunkoczi, G., Chen, V.B., Davis, I.W., Echols, N., Headd, J.J., Hung, L.W., Kapral, G.J., Grosse-Kunstleve, R.W., et al. (2010). PHENIX: a comprehensive Python-based system for macromolecular structure solution. Acta Crystallogr. D Biol. Crystallogr. *66*, 213–221.

Aghajan, M., Jonai, N., Flick, K., Fu, F., Luo, M., Cai, X., Ouni, I., Pierce, N., Tang, X., Lomenick, B., et al. (2010). Chemical genetics screen for enhancers of rapamycin identifies a specific inhibitor of an SCF family E3 ubiquitin ligase. Nat. Biotechnol. *28*, 738–742.

Angers, S., Li, T., Yi, X., Maccoss, M.J., Moon, R.T., and Zheng, N. (2006). Molecular architecture and assembly of the DDB1-CUL4A ubiquitin ligase machinery. Nature *443*, 590–593.

Figure 5. The Crystal Structures of UbV.Fl10.1 Bound Skp1-Fbl10 or Skp1-Fbl11

(A) Overall architecture of the UbV.Fl10.1-Skp1-Fbl10 and UbV.Fl10.1-Skp1-Fbl11 complexes.

(B) Open book views of contact surfaces between UbV.Fl10.1 and Skp1-Fbl10 or Skp1-Fbl11. Coloring is the same as Figure 3B, except for unengaged surfaces of Fbl10, which are colored pink.

(C) Details of the molecular interactions between UbV.Fl10.1 and Skp1-Fbl10 or Skp1-Fbl11. Dashed lines indicate hydrogen bonds. Asterisks indicate a residue from UbV.Fl10.1.

Bhowmick, P., Pancsa, R., Guharoy, M., and Tompa, P. (2013). Functional diversity and structural disorder in the human ubiquitination pathway. PLoS One *8*, e65443.

Brown, N.G., Vanderlinden, R., Watson, E.R., Weissmann, F., Ordureau, A., Wu, K.P., Zhang, W., Yu, S., Mercredi, P.Y., Harrison, J.S., et al. (2016). Dual RING E3 architectures regulate multiubiquitination and ubiquitin chain elongation by APC/C. Cell *165*, 1440–1453.

Bulatov, E., and Ciulli, A. (2015). Targeting cullin-RING E3 ubiquitin ligases for drug discovery: structure, assembly and small-molecule modulation. Biochem. J. *467*, 365–386.

Chan, C.H., Morrow, J.K., Li, C.F., Gao, Y., Jin, G., Moten, A., Stagg, L.J., Ladbury, J.E., Cai, Z., Xu, D., et al. (2013). Pharmacological inactivation of Skp2 SCF ubiquitin ligase restricts cancer stem cell traits and cancer progression. Cell *154*, 556–568.

Chen, B.B., Coon, T.A., Glasser, J.R., Mcverry, B.J., Zhao, J., Zhao, Y., Zou, C., Ellis, B., Sciurba, F.C., Zhang, Y., et al. (2013). A combinatorial F box protein directed pathway controls TRAF adaptor stability to regulate inflammation. Nat. Immunol. *14*, 470–479.

Crooks, G.E., Hon, G., Chandonia, J.M., and Brenner, S.E. (2004). WebLogo: a sequence logo generator. Genome Res. *14*, 1188–1190.

Emsley, P., and Cowtan, K. (2004). Coot: model-building tools for molecular graphics. Acta Crystallogr. D Biol. Crystallogr. *60*, 2126–2132.

Ernst, A., Avvakumov, G., Tong, J., Fan, Y., Zhao, Y., Alberts, P., Persaud, A., Walker, J.R., Neculai, A.M., Neculai, D., et al. (2013). A strategy for modulation of enzymes in the ubiquitin system. Science *339*, 590–595.

Fellouse, F.A., and Sidhu, S.S. (2007). Making antibodies in bacteria. In Making and Using Antibodies, G.C. Howard and M.S. Kaser, eds. (CRC Press), pp. 151–172.

Gabrielsen, M., Buetow, L., Nakasone, M.A., Ahmed, S.F., Sibbet, G.J., Smith, B.O., Zhang, W., Sidhu, S.S., and Huang, D.T. (2017). A general strategy for discovery of inhibitors and activators of RING and U-box E3 ligases with ubiquitin variants. Mol. Cell *68*, 456–470.e10.

Gorelik, M., Orlicky, S., Sartori, M.A., Tang, X., Marcon, E., Kurinov, I., Greenblatt, J.F., Tyers, M., Moffat, J., Sicheri, F., et al. (2016). Inhibition of SCF ubiquitin ligases by engineered ubiquitin variants that target the Cul1 binding site on the Skp1-F-box interface. Proc. Natl. Acad. Sci. USA *113*, 3527–3532.

Hoffmann, A., Kovermann, M., Lilie, H., Fiedler, M., Balbach, J., Rudolph, R., and Pfeifer, S. (2012). New binding mode to TNF-alpha revealed by ubiquitin-based artificial binding protein. PLoS One *7*, e31298.

Jin, Y., Shenoy, A.K., Doernberg, S., Chen, H., Luo, H., Shen, H., Lin, T., Tarrash, M., Cai, Q., Hu, X., et al. (2015). FBXO11 promotes ubiquitination of the Snail family of transcription factors in cancer progression and epidermal development. Cancer Lett. *362*, 70–82.

Kabsch, W. (2010). Xds. Acta Crystallogr. D Biol. Crystallogr. *66*, 125–132.

Krissinel, E., and Henrick, K. (2007). Inference of macromolecular assemblies from crystalline state. J. Mol. Biol. *372*, 774–797.

Leung, I., Jarvik, N., and Sidhu, S.S. (2017). A highly diverse and functional naive ubiquitin variant library for generation of intracellular affinity reagents. J. Mol. Biol. *429*, 115–127.

Lorey, S., Fiedler, E., Kunert, A., Nerkamp, J., Lange, C., Fiedler, M., Bosse-Doenecke, E., Meysing, M., Gloser, M., Rundfeldt, C., et al. (2014). Novel ubiquitin-derived high affinity binding proteins with tumor targeting properties. J. Biol. Chem. *289*, 8493–8507.

Manczyk, N., Yates, B.P., Veggiani, G., Ernst, A., Sicheri, F., and Sidhu, S.S. (2017). Structural and functional characterization of a ubiquitin variant engineered for tight and specific binding to an alpha-helical ubiquitin interacting motif. Protein Sci. *26*, 1060–1069.

McCoy, A.J., Grosse-Kunstleve, R.W., Adams, P.D., Winn, M.D., Storoni, L.C., and Read, R.J. (2007). Phaser crystallographic software. J. Appl. Crystallogr. *40*, 658–674.

Nangle, S., Xing, W., and Zheng, N. (2013). Crystal structure of mammalian cryptochrome in complex with a small molecule competitor of its ubiquitin ligase. Cell Res. *23*, 1417–1419.

Orlicky, S., Tang, X., Neduva, V., Elowe, N., Brown, E.D., Sicheri, F., and Tyers, M. (2010). An allosteric inhibitor of substrate recognition by the SCF(Cdc4) ubiquitin ligase. Nat. Biotechnol. *28*, 733–737.

Otwinowski, Z., and Minor, W. (1997). Processing of X-ray diffraction data collected in oscillation mode. Methods Enzymol. *276*, 307–326.

Painter, J., and Merritt, E.A. (2006). Optimal description of a protein structure in terms of multiple groups undergoing TLS motion. Acta Crystallogr. D Biol. Crystallogr. *62*, 439–450.

Pei, J., and Grishin, N.V. (2001). AL2CO: calculation of positional conservation in a protein sequence alignment. Bioinformatics *17*, 700–712.

Pettersen, E.F., Goddard, T.D., Huang, C.C., Couch, G.S., Greenblatt, D.M., Meng, E.C., and Ferrin, T.E. (2004). UCSF chimera – a visualization system for exploratory research and analysis. J. Comput. Chem. *25*, 1605–1612.

Reitsma, J.M., Liu, X., Reichermeier, K.M., Moradian, A., Sweredoski, M.J., Hess, S., and Deshaies, R.J. (2017). Composition and regulation of the cellular repertoire of SCF ubiquitin ligases. Cell *171*, 1326–1339.e14.

Schulman, B.A., Carrano, A.C., Jeffrey, P.D., Bowen, Z., Kinnucan, E.R., Finnin, M.S., Elledge, S.J., Harper, J.W., Pagano, M., and Pavletich, N.P. (2000). Insights into SCF ubiquitin ligases from the structure of the Skp1-Skp2 complex. Nature *408*, 381–386.

Skaar, J.R., Pagan, J.K., and Pagano, M. (2014). SCF ubiquitin ligase-targeted therapies. Nat. Rev. Drug Discov. *13*, 889–903.

Stogios, P.J., Downs, G.S., Jauhal, J.J., Nandra, S.K., and Prive, G.G. (2005). Sequence and structural analysis of BTB domain proteins. Genome Biol. *6*, R82.

Vijay-Kumar, S., Bugg, C.E., and Cook, W.J. (1987). Structure of ubiquitin refined at 1.8 A resolution. J. Mol. Biol. *194*, 531–544.

Wang, Y., Geer, L.Y., Chappey, C., Kans, J.A., and Bryant, S.H. (2000). Cn3D: sequence and structure views for Entrez. Trends Biochem. Sci. *25*, 300–302.

Wong, S.J., Gearhart, M.D., Taylor, A.B., Nanyes, D.R., Ha, D.J., Robinson, A.K., Artigas, J.A., Lee, O.J., Demeler, B., Hart, P.J., et al. (2016). KDM2B recruitment of the polycomb group complex, PRC1.1, requires cooperation between PCGF1 and BCORL1. Structure *24*, 1795–1801.

Wu, L., Grigoryan, A.V., Li, Y., Hao, B., Pagano, M., and Cardozo, T.J. (2012). Specific small molecule inhibitors of Skp2-mediated p27 degradation. Chem. Biol. *19*, 1515–1524.

Zhang, W., Wu, K.P., Sartori, M.A., Kamadurai, H.B., Ordureau, A., Jiang, C., Mercredi, P.Y., Murchie, R., Hu, J., Persaud, A., et al. (2016). System-wide modulation of HECT E3 ligases with selective ubiquitin variant probes. Mol. Cell *62*, 121–136.

Zhang, Y., Zhou, L., Rouge, L., Phillips, A.H., Lam, C., Liu, P., Sandoval, W., Helgason, E., Murray, J.M., Wertz, I.E., et al. (2013). Conformational stabilization of ubiquitin yields potent and selective inhibitors of USP7. Nat. Chem. Biol. *9*, 51–58.

Zheng, H., Shen, M., Zha, Y.L., Li, W., Wei, Y., Blanco, M.A., Ren, G., Zhou, T., Storz, P., Wang, H.Y., et al. (2014). PKD1 phosphorylation-dependent degradation of SNAIL by SCF-FBXO11 regulates epithelial-mesenchymal transition and metastasis. Cancer Cell *26*, 358–373.

Zheng, N., Schulman, B.A., Song, L., Miller, J.J., Jeffrey, P.D., Wang, P., Chu, C., Koepp, D.M., Elledge, S.J., Pagano, M., et al. (2002). Structure of the Cul1-Rbx1-Skp1-F boxSkp2 SCF ubiquitin ligase complex. Nature *416*, 703–709.

Zheng, N., Zhou, Q., Wang, Z., and Wei, W. (2016). Recent advances in SCF ubiquitin ligase complex: clinical implications. Biochim. Biophys. Acta *1866*, 12–22.

STAR★METHODS

KEY RESOURCES TABLE

REAGENT or RESOURCE	SOURCE	IDENTIFIER
Antibodies		
Anti-M13-HRP	GE Healthcare	Cat# 27-9421-01 RRID: AB_2616587
Anti-FLAG-HRP	Sigma	Cat# A8592 RRID: AB_439702
Mouse monoclonal anti-p27	BD Biosciences	Cat# 610241 RRID: AB_397636
Rabbit monoclonal anti-Snail (clone C15D3)	Cell Signaling	Cat# 3879 RRID: AB_2255011
Rabbit monoclonal anti-c-Myc (clone D84C12)	Cell Signaling	Cat# 5605 RRID: AB_1085878
Rabbit polyclonal anti-Cry2	Abcam	Cat# 93802 RRID: AB_2083986
Mouse monoclonal anti-Cyclin E1 (HE12)	Abcam	Cat# 3927 RRID: AB_304167
Rabbit monoclonal anti-GADPH (14C10)	Cell Signaling	Cat# 2118 RRID: AB_561053
Chemicals, Peptides, and Recombinant Proteins		
X-tremeGENE transfection reagent	Roche	Cat# 06365809001
Cycloheximide	Cell Signaling	Cat# 2112
Deposited Data		
Structure of ubiquitin refined at 1.8 Angstroms resolution	Vijay-Kumar et al., 1987	PDB ID:1UBQ
Skp1-F-box in complex with a ubiquitin variant	Gorelik et al., 2016	PDB ID: 5IBK
Structural basis for the hierarchical assembly of the core of PRC1.1	Wong et al., 2016	PDB ID: 5JH5
Crystal structure of UbV.L11.1 bound to Skp1-Fbl11	This work	PDB ID: 6BYH
Crystal structure of UbV.L10.1 bound to Skp1-Fbl10	This work	PDB ID: 6BVA
Crystal structure of UbV.L10.1 bound to Skp1-Fbl11	This work	PDB ID: 6C16
Recombinant DNA		
F-box constructs for protein expression, see Table S1	This work	N/A
p-ET-53-Dest UbV.L11.1 (N-term His-FLAG)	This work	N/A
p-ET-53-Dest UbV.L10.1 (N-term His-FLAG)	This work	N/A
p-ET-53-Dest UbV.L11.1 (N-term His-TEV)	This work	N/A
p-ET-53-Dest UbV.L10.1 (N-term His-TEV)	This work	N/A
pcDNA 3.1/nHA DEST Snail (N-term HA)	This work	N/A
pcDNA 3.1/nFlag DEST UbV.L1.1 (N-term FLAG)	This work	N/A
pcDNA 3.1/nFlag DEST UbV.O11.1 (N-term FLAG)	This work	N/A
Software and Algorithms		
GraphPad Prism 7	GraphPad	https://www.graphpad.com
Cn3D	Wang et al., 2000	https://www.ncbi.nlm.nih.gov/Structure/CN3D/cn3d.shtml
Chimera	Pettersen et al., 2004	https://www.cgl.ucsf.edu/chimera/
Origin Analysis Software	Malvern Panalytical	https://www.malvernpanalytical.com/en
Coot	Emsley and Cowtan, 2004	http://www2.mrc-lmb.cam.ac.uk/personal/pemsley/coot/
Phenix	Adams et al., 2010	http://www.phenix-online.org/
PyMol	Schrodinger	https://pymol.org/2/
Proteins, Interfaces, Structures, Assemblies (PISA)	Krissinel and Henrick, 2007	http://www.ebi.ac.uk/pdbe/pisa/
XDS	Kabsch, 2010	http://xds.mpimf-heidelberg.mpg.de/
HKL2000	Otwinowski and Minor, 1997	http://www.hkl-xray.com/

CONTACT FOR REAGENT AND RESOURCE SHARING

Further information and requests for resources and reagents should be directed to and will be fulfilled by the Lead Contact: Frank Sicheri, (sicheri@lunenfeld.ca)

EXPERIMENTAL MODEL AND SUBJECT DETAILS

Protein Expression

E. coli BL21 (DE3) cells were grown in LB medium at 37°C and proteins expressed at 16°C.

Cell Based Assays

For cell based assays human 293T cells (female) were cultured in DMEM (Gibco 11995-065) supplemented with 10% fetal bovine serum (Gibco 12483-020) and 1X Penicillin Streptomycin solution (Corning 30-002-Cl) at 37°C and 5% CO_2.

METHOD DETAILS

Protein Expression and Purification

The Skp1-F-box, UbV, and Cul1 proteins employed in phage binding selections and/or ELISAs were expressed and purified as described (Gorelik et al., 2016). Domain boundaries of F-box constructs are listed in Table S1. The Skp1-F-box-UbV complexes used in crystallization were prepared as described previously for the Skp1-F-box^{Fbw7}-Ubv.Fw7.1 complex(Gorelik et al., 2016).

Library Construction and Binding Selections

The UbV-phage library was constructed as described previously for Library 3 (Gorelik et al., 2016), except that 10-12 residues were inserted in the β1-β2 loop. The diversity of the constructed library was 1.8×10^{10}. For binding selections, GST-tagged Skp1-F-box complexes were coated on 96-well MaxiSorp plates (Thermoscientific 12565135) by adding 100 μL of 50 nM protein solution and incubating overnight at 4°C. Four rounds of binding selections with phage library pools were performed with immobilized proteins as described (Fellouse and Sidhu, 2007). To eliminate UbV-phage that bound nonspecifically, input phage pools were pre-incubated on plates coated with non-target Skp1-F-box proteins (Table S1) and the input phage pools were also mixed with 1 μM of the same non-target Skp1-F-box complex during the positive selection step. Several targets (Fbo24, Fbo28, Fbl6), which failed to generate specific UbV-phage in the initial binding selections, were subjected to a second binding selection using GST as the negative selection target.

For each Skp1-F-box target, 24-192 UbV-phage clones were screened by phage ELISA for binding to target Skp1-F-box, a non-target Skp1-F-box and with competition from Cul1. UbV-phage that exhibited >2-fold higher binding signal to target versus GST or Skp1-Fbw7, and at least 20% reduction in binding in the presence of Cul1, were further characterized. Up to 24 positive clones were sequenced from each selection (Table S2).

ELISAs

For phage ELISAs, target Skp1-F-box complexes were immobilized on 384-well MaxiSorp plates (Thermoscientific 12665347) by adding 30 μL of 50 nM protein solutions and incubating overnight at 4°C. Phage ELISAs were performed as described (Fellouse and Sidhu, 2007), except that three washes were performed for all wash steps and volumes were scaled down from 100 μL to 30 μL to accommodate the 384-well format. Binding of phage was detected using anti-M13-HRP antibody at 1:5000 dilution. For testing whether the binding of UbV-phage was inhibited by Cul1 protein, either 20 uL of PBS or 20 uL of 200 nM Cul1 were added for 10 min prior to addition of 10 uL UbV-phage. Reduction of phage-displayed Ubv binding by >20 % was considered to signify competition with Cul1 for binding. For protein ELISAs, Skp1-F-box complexes were immobilized by adding 30 μL of 200 nM protein solutions to 384-well MaxiSorp plates (Thermoscientific 12665347) and incubating overnight at 4°C. Ubv.Fl11.1 or Ubv.Fl101.1 at sub-saturating concentration were mixed with the serial dilutions of the tested Skp1-F-box complexes and applied to the plate containing immobilized Skp1-Fbl11 or Skp1-Fbl10 complexes respectively. Binding of FLAG-tagged UbV was detected using anti-FLAG-HRP antibody at 1:5000 dilution. Competitive ELISA IC_{50} values were derived from the binding curves and corresponded to the concentration of the tested Skp1-F-box complexes at which 50% of the UbV binding was observed.

Cell-Based Assays

On day 0, 6-well plates were seeded with 4×10^5 HEK293T cells. On day 1, cells were transfected with 2 μg of plasmid DNA to express FLAG-UbV using the X-tremeGENE transfection reagent according to manufacturer's protocol. For Snai1 stability assays, the cells were simultaneously transfected with 0.1 μg of plasmid DNA to express HA-tagged Snai1. On day 3, cycloheximide (100 μg/ml for p27 stability assays or 20 μg/ml for Snai1 stability assays) was added for 0-6 hours. Cells were lysed in lysis buffer (Cell Signalling 9803) and cell lysates were subjected to western blot analysis.

F-box Alignment

The alignment of F-box domains was performed using Cn3D (Wang et al., 2000). An initial structure based model of the F-box domain was performed using the F-box structures from Fbl3 (PDB:4I6J), Fbw1 (PDB:1P22), Skp2 (PDB:2ASS), Fbw7 (PDB:2OVP), Cdc4

(PDB:3MKS), and Fbl10 (PDB:5JH5). All other human F-box sequences were then imported into Cn3D and aligned using the "block align single" function. Further refinement of the alignment was done manually. Conservation was calculated using AL2C0 1.0(Pei and Grishin, 2001) in Chimera (Pettersen et al., 2004).

Crystallization and Structure Determination

The UbV.Fl11.1-Skp1-Fbl11 complex was crystallized in sitting drops at 20°C by mixing 0.2 μL protein complex (17 mg/mL) with 0.2 μL mother liquor (0.1 M PCTP buffer pH 6 and 25% w/v PEG 1500). Crystals were transferred to a cryoprotectant solution (mother liquor with 20% ethylene Glycol) and flash frozen in liquid nitrogen. A single crystal dataset was collected at -180°C on a home-source consisting of a Rigaku MicroMax-007 HF rotating anode generator coupled to a Rigaku Saturn 944 HG CCD detector. Data was processed by HKL-2000 (Otwinowski and Minor, 1997). The structure was solved by molecular replacement using Phaser(McCoy et al., 2007) and search models of Ub with the 5 C-terminal residues removed (PDB:1UBQ), Skp1 (PDB:5IBK) and Fbl10 residues 1066-1104 (PDB:5JH5). The structure was refined by PHENIX (Adams et al., 2010) using TLS parameters (Painter and Merritt, 2006) and manual building in Coot (Emsley and Cowtan, 2004).

The UbV.Fl10.1-Skp1-Fbl10 complex was crystallized in hanging drops at 20°C by mixing 1 μL protein complex (19 mg/mL) with 1 μL mother liquor (0.1 M Hepes buffer pH 7.5, 0.2 M $CaCl_2$ and 18% w/v PEG 6000). Crystals were transferred to a cryoprotectant solution (mother liquor with 20% ethylene glycol) and flash frozen in liquid nitrogen. A single crystal dataset was collected at -180°C on a PILATUS 6M-F detector at station 24-ID-C, NE CAT beamline, Advanced Photon Source (APS) and processed using HKL-2000(Otwinowski and Minor, 1997). The structure was solved by molecular replacement using Phaser (McCoy et al., 2007) and search models of ubiquitin with the 5 C-terminal residues removed (PDB:1UBQ) and Skp1-Fbl11 from our UbV.Fl11.1-Skp1-Fbl11 structure. The structure was refined by PHENIX(Adams et al., 2010) using TLS parameters (Painter and Merritt, 2006) and manual building in Coot (Emsley and Cowtan, 2004).

The UbV.Fl10.1-Skp1-Fbl11 complex was crystallized in hanging drops at 20°C by mixing 1 μL protein complex (18 mg/mL) with 1 μL mother liquor (0.1 M Malic Acid pH 4.5, 0.15 M NaCl, 27% w/v PEG 3350). Crystals were transferred to a cryoprotectant solution (mother liquor with 20% ethylene glycol) and flash frozen in liquid nitrogen. A single crystal dataset was collected at -180°C on an EIGER 16M detector at station 24-ID-C, NE CAT beamline, Advanced Photon Source (APS) and processed using XDS (Kabsch, 2010). The structure was solved by molecular replacement using Phaser (McCoy et al., 2007) and search models of Ub with the 5 C-terminal residues removed (PDB:1UBQ) (Vijay-Kumar et al., 1987) and Skp1-Fbl10 from our UbV.Fl10.1-Skp1-Fbl10 structure. The structure was refined by PHENIX (Adams et al., 2010) and manual building in Coot (Emsley and Cowtan, 2004).

Interactions for structures were analyzed manually using The PyMOL Molecular Graphics System (Schrodinger, LLC) and using the protein interfaces, surfaces and assemblies (PISA) tool (Krissinel and Henrick, 2007). Alignments were performed using Coot. Rotation and translation of structures were analyzed by the Pymol script 'RotationAxis' available on the Pymol wiki webpage. Structure representations were performed using the PyMOL molecular graphics system.

Isothermal Calorimetry

Calorimetric titrations were performed on a Malvern MicroCal Auto-iTC200 (SBC Facility at The Hospital for Sick Children) at 25°C. Protein samples were dialyzed in 300 mM NaCl, 50 mM Hepes pH 7.5, 5% glycerol, 4 mM β-mercaptoethanol. To measure UbV.Fl11.1 binding to Skp1-Fbl11, 150 μM UbV.Fl11.1 in the syringe was titrated into 20 μM Skp1-Fbl11 complex in the lower cell. To measure binding between UbV.Fl10.1 and Skp1-Fbl10 or Skp1-Fbl11, 167 μM or 150 μM UbV.Fl10.1 in the syringe was titrated into 20 μM Skp1-Fbl10 or Skp1-Fbl11 in the lower cell. Sixteen 2.49 μL injections were performed with an interval of 120 seconds.

QUANTIFICATION AND STATISTICAL ANALYSIS

Competitive ELISA Assays

IC_{50} values were calculated by fitting the obtained binding curves to four parameter logistic nonlinear regression model using GraphPad Prism software. Data represent mean ± SEM of four binding curves.

Isothermal Calorimetry Assays

Experiments were carried out in triplicate. Analysis was performed by nonlinear curve-fitting of the corrected data to a model with one site using ORIGIN software. Reported values represent the mean ± SD.

DATA AND SOFTWARE AVAILABILITY

Accession Numbers

The accession numbers for the atomic coordinates and structure factors for UbV.Fl11.1-Skp1-Fbl11, UbV.Fl10.1-Skp1-Fbl10 and UbV.Fl10.1-Skp1-Fbl11 complexes reported in this paper is PDB: 6BYH, 6BVA, 6C16.